Acta Oceanol. Sin., 2021, Vol. 40, No. 4, P. 1–9
https://doi.org/10.1007/s13131-021-1818-y
http://www.hyxb.org.cn
E-mail: ocean2@hyxb.org.cn

Response of the mixed layer depth and subduction rate in the subtropical Northeast Pacific to global warming

Ruibin Xia[1, 2*], Bingrui Li[2], Chen Cheng[3]

[1] School of Marine Sciences, Nanjing University of Information Science & Technology, Nanjing 210044, China

[2] MNR Key Laboratory for Polar Science, Po1ar Research Institute of China, Ministry of Natural Resources, Shanghai 200136, China

[3] Southern Marine Science and Engineering Guangdong Laboratory (Zhuhai), Zhuhai 519080, China

Received 22 December 2020; accepted 23 January 2021

Abstract

The response of the mixed layer depth (MLD) and subduction rate in the subtropical Northeast Pacific to global warming is investigated based on 9 CMIP5 models. Compared with the present climate in the 9 models, the response of the MLD in the subtropical Northeast Pacific to the increased radiation forcing is spatially non-uniform, with the maximum shoaling about 50 m in the ensemble mean result. The inter-model differences of MLD change are non-negligible, which depend on the various dominated mechanisms. On the north of the MLD front, MLD shallows largely and is influenced by Ekman pumping, heat flux, and upper-ocean cold advection changes. On the south of the MLD front, MLD changes a little in the warmer climate, which is mainly due to the upper-ocean warm advection change. As a result, the MLD front intensity weakens obviously from 0.24 m/km to 0.15 m/km (about 33.9%) in the ensemble mean, not only due to the maximum of MLD shoaling but also dependent on the MLD non-uniform spatial variability. The spatially non-uniform decrease of the subduction rate is primarily dominated by the lateral induction reduction (about 85% in ensemble mean) due to the significant weakening of the MLD front. This research indicates that the ocean advection change impacts the MLD spatially non-uniform change greatly, and then plays an important role in the response of the MLD front and the subduction process to global warming.

Key words: mixed layer depth, mixed layer depth front, subduction, ocean advection, non-uniform

Citation: Xia Ruibin, Li Bingrui, Cheng Chen. 2021. Response of the mixed layer depth and subduction rate in the subtropical Northeast Pacific to global warming. Acta Oceanologica Sinica, 40(4): 1–9, doi: 10.1007/s13131-021-1818-y

1 Introduction

The ocean mixed layer links the atmosphere to the deep ocean and plays a critical role in climate variability. Atmospheric fluxes of momentum, heat and freshwater through the ocean surface drive vertical mixing and provide the source of almost all oceanic motions (de Boyer Montégut et al., 2004). The ocean mixed layer is often defined as the layer where the temperature, density or vertical gradients are smaller than some values near the sea surface. So ocean mixed layer depth (MLD) is one of the most important quantities of the upper ocean as it defines the quasi-homogeneous surface region of density that directly interacts with the atmosphere (Kara et al., 2003).

There are many kinds of research about the variability and dynamics of the MLD since the last century (Levitus, 1982; Monterey and Levitus, 1997; Carton and Giese, 2008). The variability of the MLD is usually linked to many processes occurring in the mixed layer (surface forcing, ocean advection, etc.). For example, the seasonal variability of the MLD in the Kuroshio Extension is controlled by sea surface heat flux (Qiu and Kelly, 1993). Both sea surface heat flux and vertical pumping impact the mixed layer temperature seasonal variability in the three North Pacific subtropical mode water formation regions, but the contribution of ocean advection is relatively small (Pan et al., 2011). The annual and decadal variabilities of the MLD in the North Pacific are also connected with the variabilities of wind and heat flux induced by the Pacific Decadal Oscillation (Qiu and Chen, 2006; Dawe and Thompson, 2007). Previous research suggests that ocean advection could be more important than other factors for the MLD variability in some regions (Liu and Lu, 2016; Xia et al., 2018). Ocean advection changes the ocean vertical density gradient, impact the stratification, and then contribute to the ocean mixing process. Recently, some studies focus on the ocean eddy effect on MLD and they indicate that eddies could influence the winter MLD, leading to the low potential vorticity (PV) water mass change under mixed layer depth (Wang et al., 2020a; Wen et al., 2020; Xu et al., 2016). Their results also highlight the importance of the advection on the MLD changes in ocean mesoscale processes.

The response of the upper-ocean and MLD to global warming is also a significant problem. For example, the sea surface temperature (SST) change is influenced obviously by ocean advection after global warming (Xie et al. 2010). The MLD in the

Foundation item: The National Natural Science Foundation of China under contract No. 41606217; the Open Fund of the Key Laboratory of Research on Marine Hazards Forecasting under contract No. LOMF1702; the Open Fund of Key Laboratory for Polar Science, Polar Research Institute of China, Ministry of Natural Resources under contract No. KP201702; the Open Fund of the Key Laboratory of Ocean Circulation and Waves, Chinese Academy of Sciences under contract No. KLOCW1903; the Natural Science Foundation of Jiangsu Province under contract No. BK20191405.
*Corresponding author, E-mail: xiarb@nuist.edu.cn

21st century decreases in most regions of the North Pacific, whereas the spatial pattern of the MLD is nearly unchanged (Jang et al., 2011). They consider the overall shoaling results in part from intensified upper-ocean stratification caused by both surface warming and freshening. A significant MLD decrease (>30 m) is found in the Kuroshio Extension, which is predominantly driven by reduced surface cooling, caused by the weakening of wind (Jang et al., 2011). However, some subsequent researches indicate that the MLD reduction would be non-uniform and most pronounced on the southern edge of the present deep-MLD region, due to the advection of temperature change in the upper 100 m by the mean eastward flow in the models (Zhang et al., 2016). Some long-timescale observation data shows that while the SST is rising at mid-latitudes, stratification is not unequivocally increasing nor is MLD shoaling (Somavilla et al., 2017). MLD variability reveals itself as a subtle interplay between circulation and atmospheric forcing at mid-latitudes (Somavilla et al., 2017). Besides, if MLD shoals uniformly in the whole region, this change could not lead to a large change of the MLD front. The studies above have implied that other processes, such as ocean advection, may play important roles in the MLD non-uniform change process under the warmer climate.

Ocean ventilation, including the subduction and obduction process, is a key component of global oceanic circulation. Subduction and obduction have been widely used as tools describing kinematical and dynamical processes coupling the mixed layer and the ocean interior. The spatial pattern and temporal variation of the MLD both play important roles in the subduction and obduction process (Stommel, 1979; Woods, 1985; Marshall et al., 1993). Therefore, the MLD variability indirectly dominates many products caused by the subduction process, such as the mode water. Generally, sea surface net heat flux or surface wind field are considered as key factors on the MLD and then impact on the formation of the subduction rate and mode water (Hu et al., 2011; Qu and Chen, 2009; Xu et al., 2012). For example, both subantarctic mode water (SAMW) and Antarctic Intermediate Water (AAIW) are increased under intensified westerlies, increased heat loss and the lateral induction term change due to the deepening of the MLD (Liu et al., 2017). Xu et al. (2016, 2017) pointed out that PV distribution is asymmetric outside the anticyclonic eddy core, with enhanced subduction near the southeastern rim of the anticyclonic eddy. Katsura (2018) suggested the eastern subtropical mode water (ESTMW) and MLD is even related to the Pacific decadal oscillation from seasonal to interannual cycle. As the effective subduction generally occurs in late winter or early spring, when the MLD reaches its local maximum (Marshall et al., 1993), we use the February–March means to analyze the mechanism in this paper.

There are two MLD local maximum regions in the subtropical North Pacific. The previous studies usually care more about the western region with relatively deeper MLD (e.g., Jang et al., 2011; Xu et al., 2012). While the eastern MLD local maximum region, accompanied by the subduction local maximum and formation of the ESTMW, is also important. Among all the subtropical low PV water masses in North Pacific, only ESTMW and the near-equatorial North Pacific low PV water mass (NELPVW) can migrate to the equatorial Pacific, and effect subsurface oceanic temperature there (Wang et al., 2020b). Their studies provided that the MLD and subduction variation could lead to a potential climate effect near-equatorial Pacific. Due to the lack of observation data, the long-timescale variation of MLD near the ESTMW formation region is not clear. Luckily, the Coupled Model Intercomparison Project Phase 5 (CMIP5) provides us the convenience to study the long-time variability of the MLD. We indicate that the ocean heat advection plays a critical role in the banded shoaling of MLD after global warming at the ESTMW formation region (Xia et al., 2015). Although the accuracy is limited by a single model simulation. Furthermore, with the 9 CMIP5 models, we show the MLD spatial pattern in historical climate simulation in detail and suggest that the non-uniform MLD pattern causes a strong MLD front. MLD front controls the lateral induction rate pattern and then decides the non-uniform distribution of the subduction rate (Xia et al., 2018). Therefore, we provide new questions and discuss them in this paper: How does the MLD respond to global warming in models? How does the MLD front change and why? What are the characteristics and mechanisms of the inter-model differences? What influences are these inter-model differences on the subduction process? Similar to the results in previous research (Xia et al., 2015, 2018), we propose that ocean advection change affects the MLD spatially non-uniform change, and then changes the MLD front and the subduction process to the increased forcing radiation. But the inter-model differences may be non-negligible, which depend on the various dominated mechanisms.

The rest of the paper is organized as follows. A brief description of the data is introduced in Section 2. We examine the inter-model differences in the CMIP5 models, explore the mechanisms and the influence of the MLD on the subduction process in Section 3. Finally, Section 4 shows the summary and discussion.

2 Data and methods

The present study primarily uses the output from the 9 global coupled climate models (Table 1) as part of the CMIP5 (Dunne et al., 2012; Taylor et al., 2012). We choose the historical simulation and the Representative Concentration Pathways (RCP) 8.5 scenario. The historical simulation simulates the 20th century climate forced by observed atmospheric composition changes. While in the RCP8.5 scenario, the radiative forcing increases throughout the 21st century before reaching a level of approximately 8.5 W/m^2 at the end of the century respectively (Taylor et al., 2012). The present-day mean state is taken from 1951 to 2000 in the historical simulation and the future climatology is from 2051 to 2100 in the RCP8.5 scenarios. Fifty-year averaged variables in those scenarios are calculated to represent

Table 1. The 9 models from CMIP5 analyzed in this study

Model	Institution	Country
CCSM4	National Center for Atmospheric Research	USA
CNRM-CM5	Centre National de Recherches Meteorologiques	France
GFDL-ESM2G	NOAA/Geophysical Fluid Dynamics Laboratory	USA
GFDL-ESM2M	NOAA/Geophysical Fluid Dynamics Laboratory	USA
IPSL-CM5A-LR	Institute Pierre-Simon Laplace	France
IPSL-CM5A-MR	Institute Pierre-Simon Laplace	France
MIROC-ESM	University of Tokyo	Japan
MPI-ESM-LR	Max Planck Institute for Meteorology	Germany
MRI-CGCM3	Meteorological Research Institute	Japan

their mean state, and the variabilities between the historical and RCP8.5 scenarios represent the changes in global warming.

The spatial resolution varies between models and within the same model for atmospheric and oceanic variables. To facilitate comparison with each model and observations, we interpolated them onto a 1°×1° latitude-longitude grid. We investigate both the common features (ensemble mean) and the inter-model differences among models, focusing on the MLD variability and dynamics. The same member run (R1i1p1) is chosen in all models. The model outputs are freely available from the Program for Climate Model Diagnosis and Intercomparison (PCMDI) at the Lawrence Livermore National Laboratory (http://cmip-pcmdi.llnl.gov/cmip5/). The model in historical simulation has been examined with the Levitus-94 data (Levitus and Boyer, 1994) and Argo data (Xia et al., 2018). These data are both 1°×1° gridded and from the Asia-Pacific Data Research Center (APDRC, http://apdrc.soest.hawaii.edu/).

3 Results

3.1 *The response of the subtropical northeast Pacific MLD to increased radiation forcing*

Single model simulation indicated that the MLD during February–March is banded shoaling in response to global warming, with a maximum shoaling of 50 m, leading to the lateral induction reduction (Xia et al., 2015). While more model simulation results (Fig. 1) indicate that the above conclusion may depend on the chosen model. In the RCP8.5 scenario experiments, all models show the MLD shoaling pattern in this region.

As shown in Fig. 1, the contours indicate the mean MLD difference (RCP8.5 minus historical), as the dashed lines (negative values) means the MLD shoals in a much warmer climate. MLD shoals in all models, which is similar to the single model result (Xia et al., 2015). But the MLD change pattern is relatively diverse in different models. We will discuss these similarities and differences in detail next, which will influence the MLD front change pattern directly. The MLD horizontal gradient h_{grad} is calculated as

$$h_{\mathrm{grad}} = \nabla h_{\mathrm{m}} = \frac{\partial h_{\mathrm{m}}}{\partial x}\vec{i} + \frac{\partial h_{\mathrm{m}}}{\partial y}\vec{j}, \tag{1}$$

where the unit of h_{grad} is m/km. In this paper, we use MLD front intensity to represent the MLD horizontal gradient maximum.

MLD in historical simulation (shading in Fig. 1) in all models show an inter-regional diversity, which is much deeper (>140 m) in the northern region and relatively shallower (<60 m) in the southern region. Thus we divide this area into two regions, while the MLD fronts (magenta points in Fig. 1) are suitable boundaries. The two regions are called "northern region" (north of the MLD front) and "southern region" (south of the MLD front) respectively (Xia et al., 2018). When concerned with the response of MLD (contours in Fig. 1) to the warmer climate, it is obvious that the MLD change is also divided by these boundaries in almost all models (except MRI-CGCM3). The MLD shoals more in the northern region, where the MLD maximum exists in historical simulation. The MLD maximum shoals over 30 m with increased radiation forcing in the ensemble mean result of the 9 CMIP5 models. As a result, the MLD front intensity weakens obviously from 0.24 m/km to 0.15 m/km (weakened by 33.9%). While with shallower MLD in historical simulation, the MLD change is much smaller in the southern region than that in the

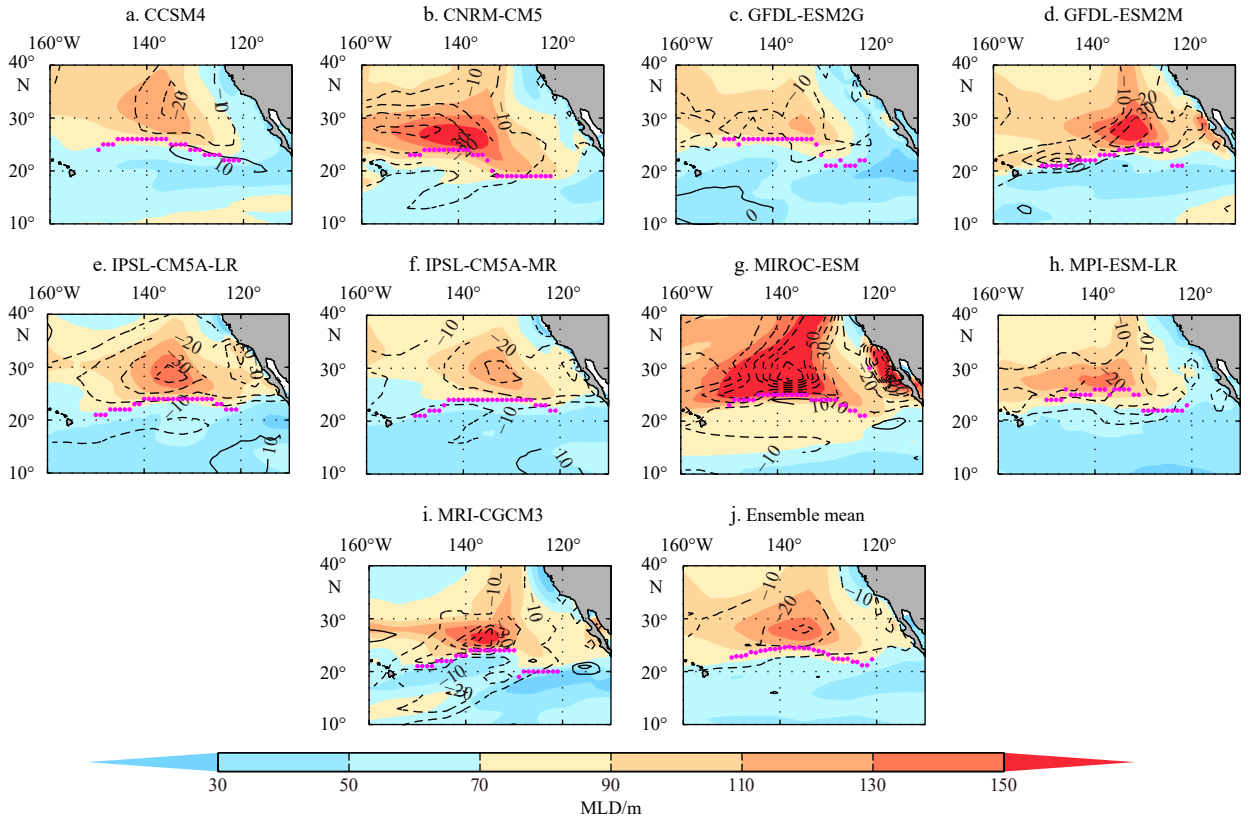

Fig. 1. The February–March mean MLD (shading, interval: 20 m) from the historical simulation of the 9 models (a–i) and ensemble mean result (j). The contours indicate the mean MLD difference (RCP8.5 minus historical), dashed lines (negative values) means the MLD shoals in a much warmer climate. Magenta points represent the location of the MLD front in historical simulation.

northern region. Especially, the MLD even slightly deepened in CCSM4, MIROC-ESM in the southern region. In other words, it seems that the deeper of MLD in historical simulation, the shallower after increased forcing radiation. The ensemble mean also reflects this characteristic. This non-uniform MLD change pattern is highly consistent with the non-uniform MLD pattern in historical simulation (Figs 1 and 2a), which significantly reduces the MLD front intensity. As shown in Fig. 2, the decrease of the MLD front (33.9%) is generally larger than the shoaling of MLD (22.2%) in the MLD maximum region.

The MLD change pattern (contours in Fig. 1) is non-uniform and its inter-model differences could not be ignored. This phenomenon indicates it is not accurate to discuss the mechanism with only one model. The inter-model differences mainly reflect in the following two aspects. First, in the northern region, though the MLD shoals larger than that in the southern region in all models, the maximum of MLD shoaling differs considerably in different models (Fig. 2a). The maximum of MLD shoaling is only about 20–30 m in CCSM4, IPSL-CM5A-MR, but increasing to 40–50 m in CNRM-CM5, GFDL-ESM2M, and arriving at the maximum 80 m in MIROC-ESM. Compared with the MLD in historical simulation, it is easy to find that the deeper of MLD in historical simulation, the shallower after increased forcing radiation. This characteristic occurs not only in the diverse regions in one model but also in the inter-model differences. Generally, the weakening magnitude of the MLD front is consistent with the shoaling of the MLD maximum. But the MLD front is weakened to the maximum in MRI-CGCM3, in which there is not the largest MLD shoaling maximum. Second, in the southern region, the MLD shoals small in all models RCP8.5 scenario experiments. But the changing pattern could be divided into two categories. First, although the shoaling magnitude and location are not consistent, a banded shoaling from southwest to northeast could be found in CNRM-CM5, GFDL-ESM2M, MPI-ESM-LR and MRI-CGCM3, similar to the previous research (Xia et al., 2015). Second, the MLD is shallowed a little or even deepened in some regions in the rest of the 5 models.

In summary, the MLD change pattern (contours in Fig. 1) is non-uniform and its inter-model differences could not be ignored. Both the consistency of the models and the inter-model differences show that the change of MLD front is not only due to the maximum of MLD shoaling but also depended on the MLD non-uniform spatial variability. As a result, the decrease of the MLD front (33.9%) is generally larger than the shoaling of MLD (22.2%) in the MLD maximum region (Fig. 2). This result indicates that the subduction process may become much weaker, also depended on the MLD non-uniform spatial variability. We will discuss this question in Section 3.3.

3.2 *Mechanisms of the MLD front change*

The inter-model differences in both regions suggest that dominant factors of the MLD change depend on the models or regions. In this part, we will focus on these mechanisms. The response of dominant factors is various in the 9 models, due to variable regions, the external forcing, or parameterization designs. To discuss the influence of these factors clearly, we still use the two regions divided by the MLD front: the northern region and the southern region. Comparing these models, we could get more information about how do these factors influence the MLD change and which factor plays a dominant role in the long-time scales of the MLD change process.

In the historical simulation, the spatial pattern of the Ekman pumping caused by sea surface wind stress is generally similar in all models and contributes to the winter MLD deepening in almost the whole region (Xia et al., 2018). However, compared with the RCP8.5 experiment, the Ekman pumping change patterns are disordered and inconsistent in different models (Fig. 3). Though

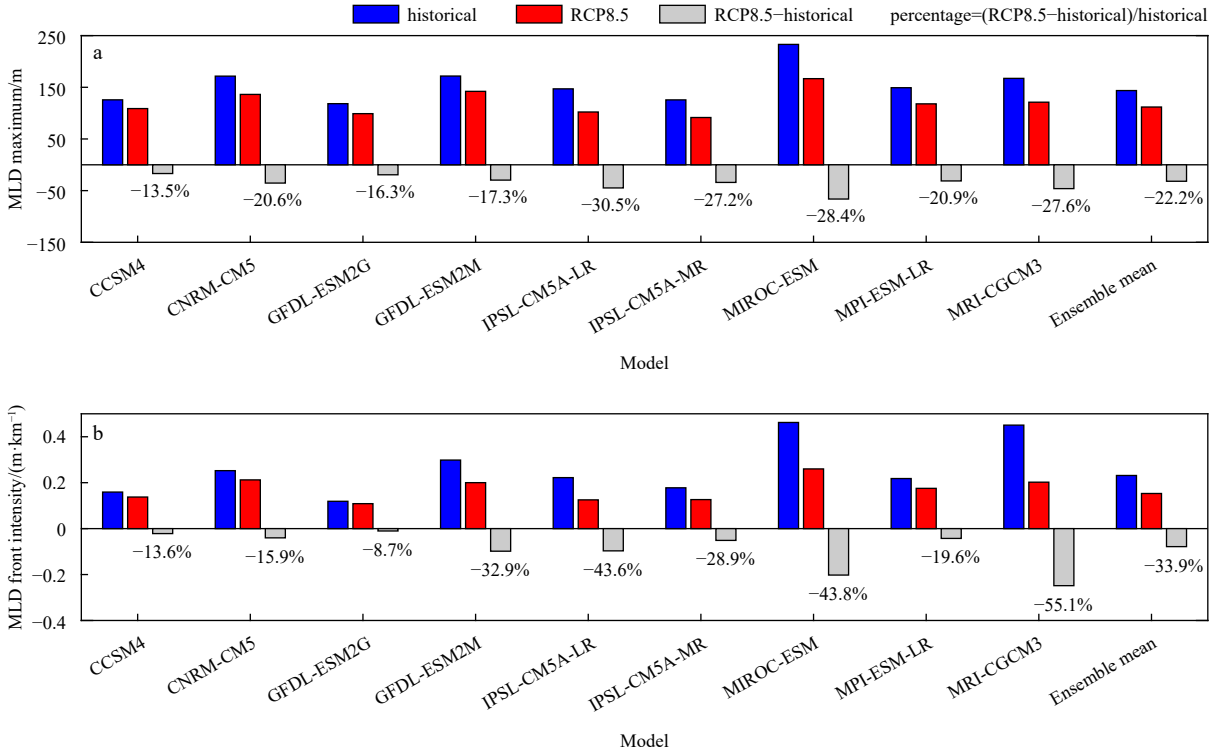

Fig. 2. The MLD maximum (a), the intensity of the MLD front mean (b) during February–March in the 9 CMIP5 models and ensemble mean result. The colors represent historical simulation (blue), RCP8.5 experiment (red), and their differences (gray). Percentages represent changes compared to corresponding historical simulation.

the weakened Ekman pumping could make a positive contribution to the MLD shoaling in most models, the Ekman pumping change locations are not corresponding with the MLD change patterns. For example, the maximum locations of Ekman pumping weakening are far away from the MLD shoaling maximum cores in IPSL-CM5A-LR, IPSL-CM5A-MR, and MIROC-ESM.

Similar to Ekman pumping, the ocean releases heat flux to the atmosphere in all models and contributes to the winter MLD deepening spatial quite uniformly in the historical simulation (Xia et al., 2018). But the change of heat flux in a warmer climate is also relatively variable in those models. In the northern region, the ocean releases less heat in CCSM, CNRM-CM5, GFDL-ESM2G, and GFDL-ESM2M, which is consistent with the MLD shoaling; but releases more heat and blocks MLD shoaling in other models. In the southern region, the inter-model differences of heat flux change influence are also huge (see details in Table 2 and Fig. 4). Noticed that is interesting for the net heat flux change in MRI-CGCM3: the ocean releases more heat to the atmosphere in all regions after global warming. This change of heat flux provides a negative contribution and impedes the shoaling of MLD in the whole region.

The inter-model differences in upper-ocean temperature advection are also significant (Fig. 5). In the northern region, there is southward cold advection to contribute to the MLD deepening in historical simulation (Figs 5 and 6 in Xia et al., 2018). With increased radiation forcing, the cold advection is weakened in CCSM4, GFDL-ESM2M and MPI-ESM-LR, increased in CNRM-CM5, IPSL-CM5A-LR, IPSL-CM5A-MR and MRI-CGCM3, and changed little in the other two models. Compared with the changes of Ekman pumping and net heat flux, it is indicated that the cold ocean advection change contributes to the MLD shoaling mainly in CCSM4 and GFDL-ESM2M, and even plays the dominant role in MPI-ESM-LR in the northern region. In the southern region, the historical warm advection (Figs 5 and 6 in Xia et al., 2018) is strengthened in CNRM-CM5, GFDL-ESM2M, MPI-ESM-LR, and MRI-CGCM3, which is highly consistent with the MLD shoaling. In other models, warm advection reduces and helps to deepen the MLD in the southern region, especially in GFDL-ESM2G, IPSL-CM5A-LR, and IPSL-CM5A-MR.

Because the inter-model differences are non-negligible, the ensemble mean is unrepresentative (Table 2). As mentioned in Section 3.1, we divided this area into the northern region and southern region by the MLD front. In the northern region, decreasing Ekman pumping dominates the MLD shoaling in IPSL-CM5A-LR, IPSL-CM5A-MR, and MRI-CGCM3. The ocean releases less heat flux to the atmosphere and plays the most important role in CNRM-CM5, MPI-ESM-LR. Only cold advection contributes to the MLD shoaling in MPI-ESM-LR. While in CCSM4 and GFDL-ESM2M, both the changes in heat flux and ocean cold advection are consistent with the MLD shoaling pattern.

As for the southern region, we defined two categories to distinguish the inter-model differences of the MLD change pattern in Section 3.1. In CNRM-CM5, GFDL-ESM2M, MPI-ESM-LR, and MRI-CGCM3, there are MLD banded shoaling from southwest to northeast, which is highly corresponding to the increasing upper-ocean warm advection. Upper-ocean warm advection contributes to strength the stratification and reduces the mixing. On the contrary, MLD changes little or even deepens in the other areas and the other 5 models. In these regions, the ocean advection change is negative. As the ocean advection is basically warm advection caused by Ekman advection in historical simulation (Xia

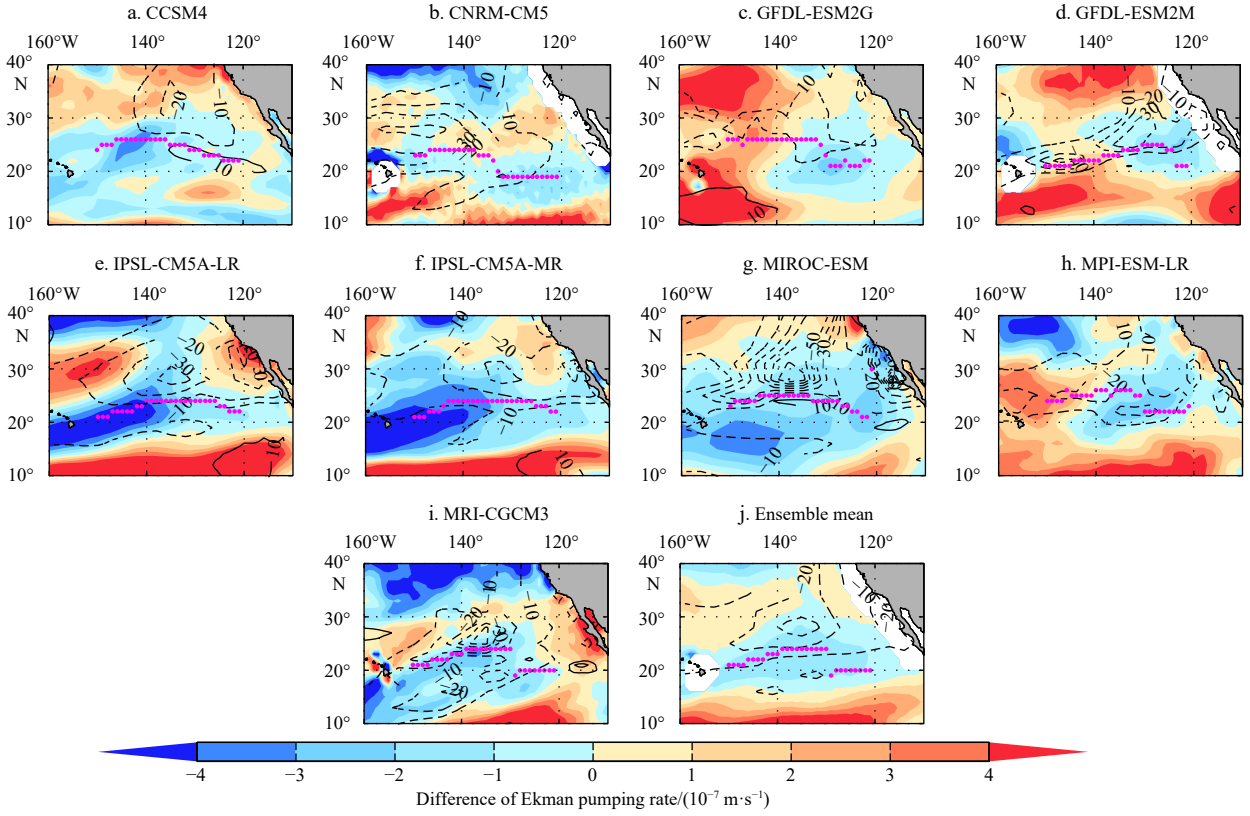

Fig. 3. Differences (RCP 8.5 minus historical) of Ekman pumping rate (shading, downward is positive) mean during February–March of the 9 models (a–i) and ensemble mean result (j). The positive values indicate the Ekman pumping trend to downward and contribute to deepening the MLD. The contours indicate the difference (RCP8.5 minus historical) in MLD mean during February–March (contours, interval: 10 m). The magenta points represent the location of the MLD front in historical simulation.

Table 2. Qualitative comparison of the contribution of the three major factors to MLD change after global warming

ID	Model	Northern region				Southern region			
		Contribution of factor			MLD trend	Contribution of factor			MLD trend
		w_e	Q	T_{ad}		w_e	Q	T_{ad}	
a	CCSM4	+	−	−	↓	+	+	+	↑
b	CNRM-CM5	+	−	+	↓	+	−	−	↓
c	GFDL-ESM2G	+	−	+	↓	+	+	+	↑
d	GFDL-ESM2M	+	−	−	↓	+	+	−	↓
e	IPSL-CM5A-LR	−	+	+	↓	−	−	+	↑
f	IPSL-CM5A-MR	−	+	+	↓	−	−	+	↑
g	MIROC-ESM	−	+	−	↓	−	+	−	↓
h	MPI-ESM-LR	+	+	−	↓	+	+	−	↓
i	MRI-CGCM3	−	+	+	↓	−	+	−	↓

Note: w_e, Q, and T_{ad} represent the Ekman pumping, net heat flux, and upper-ocean heat advection, respectively; + means it contributes to the MLD deepening, while − means it helps to shallow the MLD; the red color represents that factor is dominant to the actual MLD change; MLD trend represents the final change of MLD, ↑ means the MLD deepened, and ↓ means the MLD shallowed.

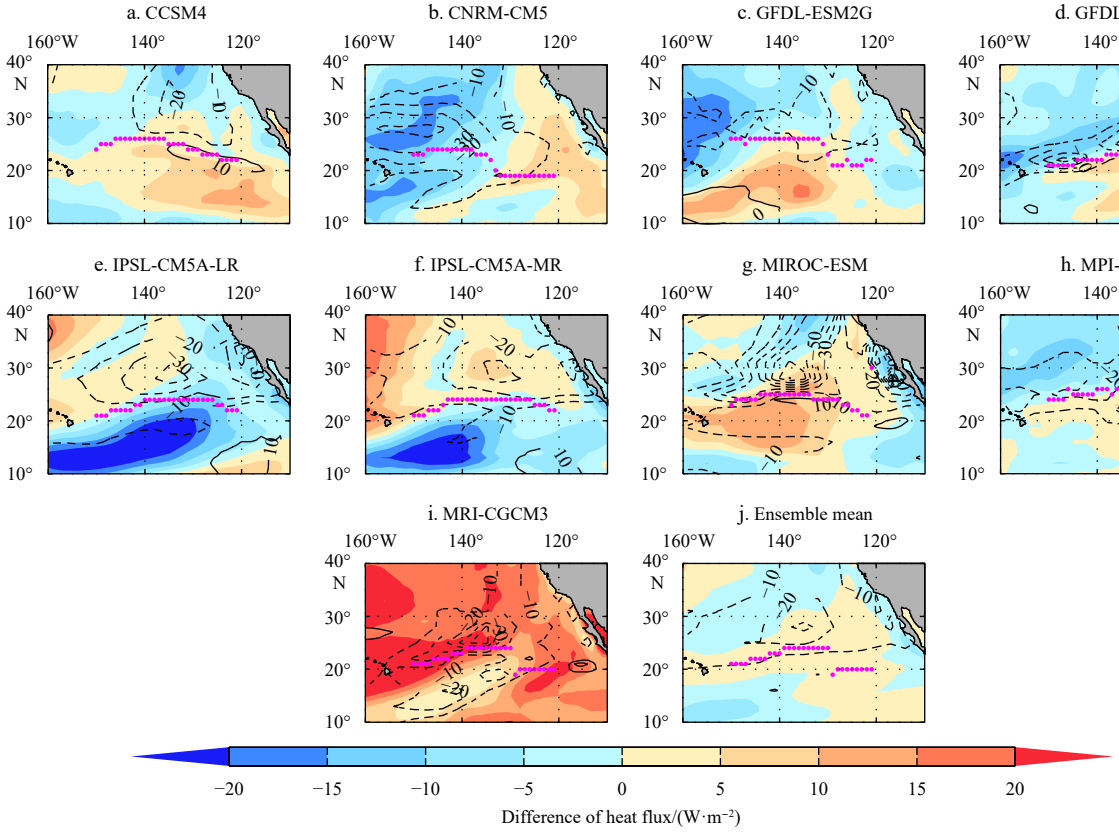

Fig. 4. Differences (RCP 8.5 minus historical) of heat flux (shading) mean during February–March of the 9 models (a–i) and ensemble mean result (j). The positive values indicate the ocean release more heat to the atmosphere and contribute to deepening the MLD. The contours indicate the difference (RCP8.5 minus historical) in MLD mean during February–March (contours, interval: 10 m). The magenta points represent the location of the MLD front in historical simulation.

et al., 2018). Therefore, the negative change means that the warm advection decreases and contributes to weakening the stratification and then deepening the MLD. Both above categories suggest that ocean advection change plays a key role in maintaining the MLD in the southern region. Our previous research has demonstrated that the shoaling contribution of the warm ocean advection could offset the deepening contribution of heat flux and Ekman pumping (Xia et al., 2018). This mechanism also works on the MLD change in RCP8.5 experiments.

In conclusion, the inter-model differences are non-negligible and the dominant mechanisms of MLD change are quite diverse in individual regions or models. For the northern region, MLD shallow greatly and is influenced by the above three factors. The contribution proportions of these factors generally change due to the various models. For the southern region, MLD changes a little under the warmer climate, when the ocean becomes warmer and stratification is strengthened. In some models, there are MLD banded shoaling regions. Both situations in the southern region are mainly due to the upper ocean warm advection change, caused by the change of trade wind. Although large inter-model differences exist in other factors, the change of ocean advection is truly similar in all the models. The less shoaling of MLD in the southern region combines with obviously shoaling of MLD in the northern region, and then causes the significant weakening of the MLD front.

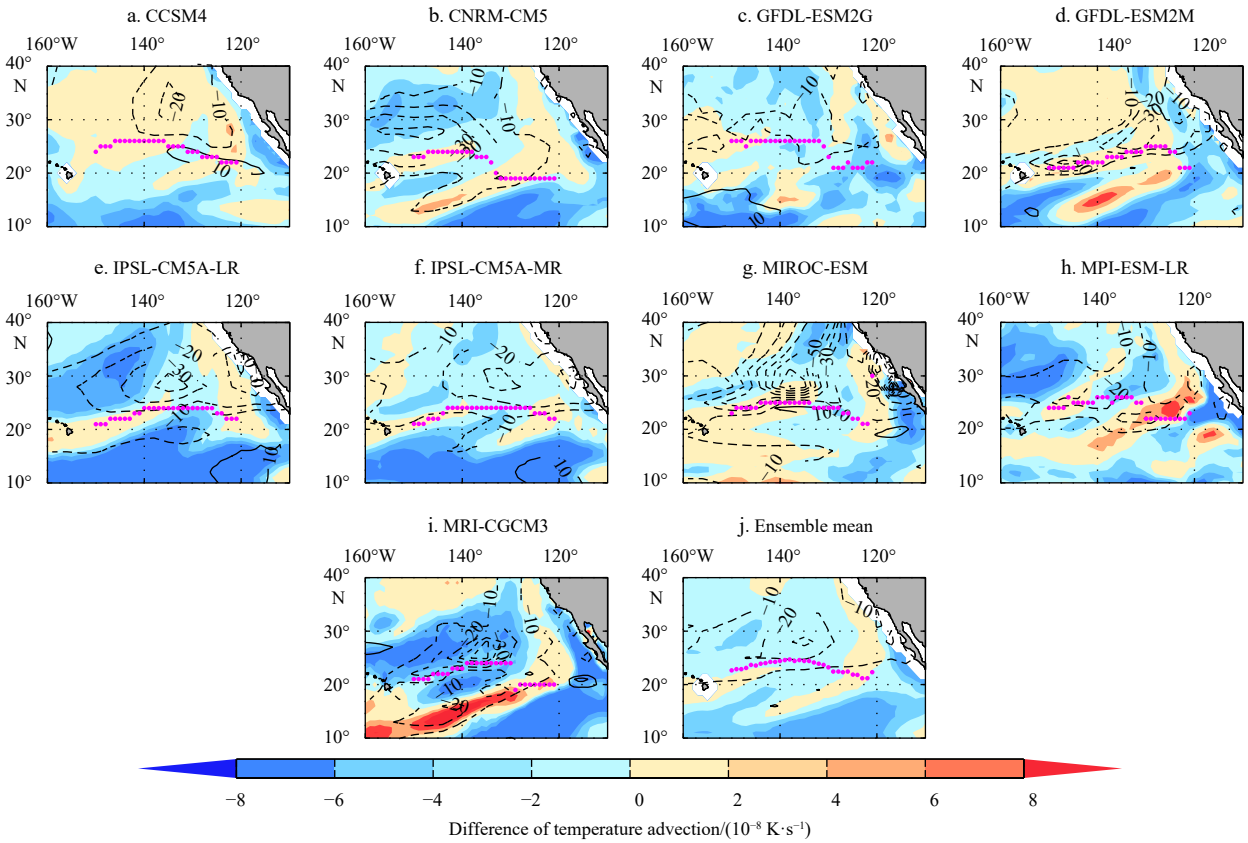

Fig. 5. Differences (RCP 8.5 minus historical) of temperature advection (shading) mean during February–March of the 9 models (a–i) and ensemble mean result (j). The positive values indicate warm advection increased or cold advection decreased in the upper ocean and contribute to shoaling the MLD. The contours indicate the difference (RCP8.5 minus historical) in MLD mean during February–March (contours, interval: 10 m). The magenta points represent the location of the MLD front in historical simulation.

3.3 *The influence of the MLD front change on the subduction*

The subduction rate is defined as (Williams, 1991; Xu et al., 2012):

$$S_{\text{mean}} = -\vec{u_{\text{m}}} \cdot \nabla h_{\text{m}} + w_{\text{e}}, \tag{2}$$

where $-\vec{u_{\text{m}}} \cdot \nabla h_{\text{m}}$ is the lateral induction, occurs at the current across the front of the MLD. The Ekman pumping velocity w_{e} can be defined as $w_{\text{e}} = \text{curl}_z(\tau/f)/\rho_0$ (Pond and Pickard, 1983), where τ is the wind stress and f is the Coriolis parameter. As the effective subduction only occurs after the MLD reaches a maximum, we calculate the subduction rate during February–March from Eq. (2). The subduction rate maximum spatial patterns are similar in the 9 models in historical simulation (Fig. 6, contours). In the ensemble mean, the subduction maximum region forms a banded structure near the east-west direction, with the maximum 4×10^6 m/s at (24°N, 140°W). Previous research suggests this non-uniform subduction rate spatial pattern is almost dominated by the non-uniform lateral induction rate distribution (Xia et al., 2018). The latter is highly consistent with the position and intensity of the MLD front.

In a warmer climate, subduction decreases in almost all the models (Fig. 6). In the ensemble mean, the subduction maximum changes from 3.03×10^{-6} m/s to 2.55×10^{-6} m/s, weakening about 0.48×10^{-6} m/s (15.7%). Surprisingly, the subduction decreasing maximum regions in all models is highly consistent with the historical subduction maximum regions, where is actually the source regions of ESTMW in historical simulation. Therefore, the reduction of subduction maximum pushes less water into the thermocline and leads to less mode water formation as a result directly. In the warmer climate, the lateral induction change caused by the MLD front change is still the dominant factor of the subduction change. In the ensemble mean, the lateral induction rate decreases by 0.4×10^6 m/s (about 29.1%) after global warming, and provides more than 85% of contribution to the subduction change. That is why the location of subduction decreasing is highly consistent with the historical MLD front (Fig. 6) in almost all the models.

The inter-model difference of subduction is mainly caused by the inter-model difference of lateral induction (Xia et al., 2018). Comparing the historical simulation with the RCP8.5 scenario, we find inter-model differences still exist in the changes of subduction and lateral induction, but not as big as the MLD change factors mentioned in Section 3.2. A possible reason is that whichever controls the MLD change, the final result is to weaken the MLD front, and then impact on subduction. It is conspicuous that the lateral induction change is larger in GFDL-ESM2M, MPI-ESM-LR, MIROC-ESM, and MRI-CGCM3 (almost over 20%) than that in other models (Fig. 6), corresponding with the inter-model differences of MLD front intensity change (Fig. 2b). In other words, ocean advection seems almost the dominant factor in these four models (Table 2).

4 Summary and discussion

The objective of this study is to describe the possible response of the MLD and the subduction process after global warming and discuss the mechanisms. Comparing with the his-

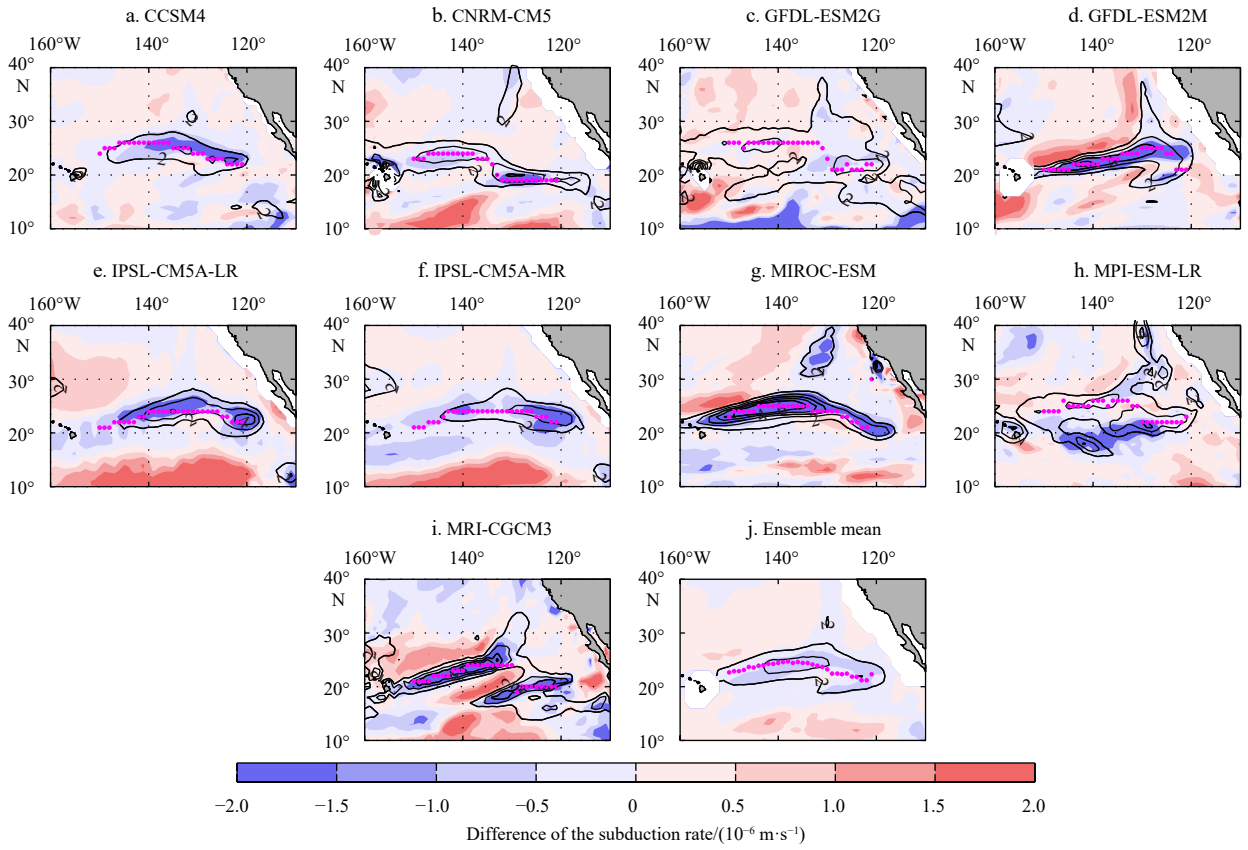

Fig. 6. Differences (RCP 8.5 minus historical) of the subduction rate (shading, downward is positive) and subduction in historical simulation (contours, only over 2×10^6 m/s are shown) during February–March in the 9 models (a–i) and ensemble mean (j) result. The magenta points represent the location of the MLD front in historical simulation.

torical simulation and RCP8.5 experiment in 9 CMIP5 models, we find the MLD change pattern is non-uniform and its inter-model differences could not be ignored. The change of MLD front is not only due to the maximum of MLD shoaling, but also depended on the MLD non-uniform spatial variability. In the ensemble mean, the decrease of the MLD front is about 1.5 times as large as the shoaling of MLD maximum. As a result, the weekened subduction is mainly caused by the decreased lateral induction, while the latter comes from the MLD front reduction. In the ensemble mean, the lateral induction rate decreases by 0.4×10^6 m/s (about 29.1%), and provides more than 85% of contribution to the subduction change. To see a single model, the lateral induction change is larger in GFDL-ESM2M, MPI-ESM-LR, MIROC-ESM, and MRI-CGCM3 (almost over 20%) than that in other models, corresponding with the larger MLD front intensity change, where ocean advection is almost the dominated factor. Xu et al. (2012) found that the low PV water and Subtropical Countercurrent (STCC) first show a sharp weakening trend when the radiative forcing increases, but then reverse to a slow strengthening trend of smaller magnitude after the radiative forcing is stabilized. This is because the subsequent warming is greater at the subsurface than that at the sea surface, destabilizing the upper ocean and becoming favorable for the low PV water formation. Their result better supports our conclusion, because they used the RCP4.5 scenario to simulate the warmer climate and the concern region (western Pacific) also differs from ours. The radiative forcing is increased sharply to 4.5 W/m^2 and then keeps stable in the RCP4.5 scenario (van Vuuren et al., 2011). But the radiative forcing maintains a linear growth in RCP8.5 (van Vuuren et al., 2011), which means the ocean fast response is not finished until 2100. This continually growing radiative forcing and the inter-regional difference may be the key reasons for MLD decreasing in this paper.

The inter-model differences of MLD change are non-negligible, which rely on the variable dominant mechanisms in various regions or models. For the northern region, MLD shallows greatly and is influenced by all the three factors mentioned above. The contribution proportions of these factors are generally diverse among regions and models. In the southern region, MLD becomes a little deepening or slight banded shoaling. Both situations in the southern region are mainly due to the upper ocean warm advection change, caused by the change of trade wind. Although the inter-model differences of Ekman pumping and heat flux changes are large, the change of ocean advection in the southern region is quite similar in all the models. The less shoaling of MLD in the southern region combines with obviously shoaling of MLD in the northern region, leading to the significant weakening of the MLD front. As we know, climate change is affected by all kinds of forcings, and the individual climate effects of each force are difficult to analyze. A quantitative diagnostic is necessary for further work. Liang-Kleeman information flow method may be one useful method to establish a causal relationship (Jiang et al., 2019).

Compared with observation data, the simulated MLD in models is usually deeper and non-uniform in the spatial pattern. Both amplified MLD front intensity and the lack of eddy dissipation cause larger subduction in CMIP5 models. As a result, mode water can be generated in a wider region and the low vorticity can be maintained and extended far to the south. In recent years, more and more researchers begin to focus on the eddy effects on

the subduction and the mode water formation. It is found that eddy activities contribute to the MLD variation in various time scales (days to years), and then impact the subduction process in many regions (Wang et al., 2020a; Wen et al., 2020; Xu et al., 2016, 2017). With the development of high-resolution models in CMIP6, exploring the eddy effect in decadal to multi-annual cycles in a warmer or colder climate becomes realizable, which will be carried out in our future research.

Acknowledgements

We appreciate the World Climate Research Programme's Working Group on Coupled Modeling, which is responsible for CMIP5. We thank the climate modeling groups (as listed in Table 1) for producing and making available their model output.

References

Carton J A, Giese B S. 2008. A reanalysis of ocean climate using Simple Ocean Data Assimilation (SODA). Monthly Weather Review, 136(8): 2999–3017, doi: 10.1175/2007MWR1978.1

Dawe J T, Thompson L A. 2007. PDO-related heat and temperature budget changes in a model of the North Pacific. Journal of Climate, 20(10): 2092–2108, doi: 10.1175/JCLI4229.1

de Boyer Montégut C, Madec G, Fischer A S, et al. 2004. Mixed layer depth over the global ocean: An examination of profile data and a profile-based climatology. Journal of Geophysical Research: Oceans, 109(C12): C12003, doi: 10.1029/2004JC002378

Dunne J P, John J G, Adcroft A J, et al. 2012. GFDL's ESM2 global coupled climate-carbon earth system models: Part I, Physical formulation and baseline simulation characteristics. Journal of Climate, 25(19): 6646–6665, doi: 10.1175/JCLI-D-11-00560.1

Hu Haibo, Liu Qinyu, Zhang Yuan, et al. 2011. Variability of subduction rates of the subtropical North Pacific mode waters. Chinese Journal of Oceanology and Limnology, 29(5): 1131–1141, doi: 10.1007/s00343-011-0237-x

Jang C J, Park J, Park T, et al. 2011. Response of the ocean mixed layer depth to global warming and its impact on primary production: a case for the North Pacific Ocean. ICES Journal of Marine Science, 68(6): 996–1007, doi: 10.1093/icesjms/fsr064

Jiang Shunyu, Hu Haibo, Zhang Ning, et al. 2019. Multi-source forcing effects analysis using Liang–Kleeman information flow method and the community atmosphere model (CAM4.0). Climate Dynamics, 53(9): 6035–6053

Kara A B, Rochford P A, Hurlburt H E. 2003. Mixed layer depth variability over the global ocean. Journal of Geophysical Research: Oceans, 108(C3): 3079, doi: 10.1029/2000JC000736

Katsura S. 2018. Properties, formation, and dissipation of the North Pacific eastern Subtropical Mode Water and its impact on interannual spiciness anomalies. Progress in Oceanography, 162: 120–131, doi: 10.1016/j.pocean.2018.02.023

Levitus S E. 1982. Climatological atlas of the World Ocean. NOAA Professional Paper 13. Washington DC: US Government Printing Office

Levitus S, Boyer T P. 1994. World Ocean Atlas 1994. Vol. 4. Temperature. Washington, DC: National Environmental Satellite, Data, and Information Service

Liu Qinyu, Lu Yiqun. 2016. Role of horizontal density advection in seasonal deepening of the mixed layer in the subtropical Southeast Pacific. Advances in Atmospheric Sciences, 33(4): 442–451, doi: 10.1007/s00376-015-5111-x

Liu Chengyan, Wang Zhaomin, Li Bingrui, et al. 2017. On the response of subduction in the South Pacific to an intensification of westerlies and heat flux in an eddy permitting ocean model. Advances in Atmospheric Sciences, 34(4): 521–531, doi: 10.1007/s00376-016-6021-2

Marshall J C, Williams R G, Nurser A J G. 1993. Inferring the subduction rate and period over the North Atlantic. Journal of Physical Oceanography, 23(7): 1315–1329, doi: 10.1175/1520-0485(1993)023<1315:ITSRAP>2.0.CO;2

Monterey G I, Levitus S. 1997. Climatological cycle of mixed layer depth in the world ocean. NOAA Atlas NESDIS 14. Washington, DC: US Government Printing Office

Pan Aijun, Wan Xiaofang, Liu Qinyu. 2011. Diagnostics of mixed-layer thermodynamics in the formation regime of the North Pacific subtropical mode water. Journal of Tropical Oceanography (in Chinese), 30(5): 8–18

Pond S, Pickard G L. 1983. Introductory Dynamical Oceanography. 2nd ed. New York: Pergamon, 379

Qiu Bo, Chen Shuming. 2006. Decadal variability in the formation of the North Pacific Subtropical mode water: Oceanic versus atmospheric control. Journal of Physical Oceanography, 36(7): 1365–1380, doi: 10.1175/JPO2918.1

Qiu Bo, Kelly K A. 1993. Upper-ocean heat balance in the Kuroshio extension region. Journal of Physical Oceanography, 23(9): 2027–2041, doi: 10.1175/1520-0485(1993)023<2027:UOHBIT>2.0.CO;2

Qu Tangdong, Chen Ju. 2009. A North Pacific decadal variability in subduction rate. Geophysical Research Letters, 36(22): L22602, doi: 10.1029/2009GL040914

Somavilla R, González-Pola C, Fernández-Diaz J. 2017. The warmer the ocean surface, the shallower the mixed layer. How much of this is true?. Journal of Geophysical Research: Oceans, 122(9): 7698–7716, doi: 10.1002/2017JC013125

Stommel H. 1979. Determination of water mass properties of water pumped down from the Ekman layer to the geostrophic flow below. Proceedings of the National Academy of Sciences of the United States of America, 76(7): 3051–3055, doi: 10.1073/pnas.76.7.3051

Taylor K E, Stouffer R J, Meehl G A. 2012. An overview of CMIP5 and the experiment design. Bulletin of the American Meteorological Society, 93(4): 485–498, doi: 10.1175/BAMS-D-11-00094.1

van Vuuren D P, Edmonds J, Kainuma M, et al. 2011. The representative concentration pathways: An overview. Climatic Change, 109(1): 5

Wang Ran, Cheng Xuhua, Xu Lixiao, et al. 2020a. Mesoscale eddy effects on the subduction of North Pacific eastern subtropical mode water. Journal of Geophysical Research: Oceans, 125(5): e2019JC015641

Wang Ziyi, Wen Zhibin, Hu Haibo, et al. 2020b. The characteristics of near - equatorial North Pacific Low PV water and its possible influences on the Equatorial Subsurface Ocean. Journal of Geophysical Research: Oceans, 125(9): e2020JC016282

Wen Zhibin, Hu Haibo, Song Zhenya, et al. 2020. Different influences of mesoscale oceanic eddies on the North Pacific subsurface low potential vorticity water mass between winter and summer. Journal of Geophysical Research: Oceans, 125(1): e2019JC015333

Williams R G. 1991. The role of the mixed layer in setting the potential vorticity of the main thermocline. Journal of Physical Oceanography, 21(12): 1803–1814, doi: 10.1175/1520-0485(1991)021<1803:TROTML>2.0.CO;2

Woods J D. 1985. The physics of pycnocline ventilation. In: Nihoul J C J, ed. Coupled Ocean-Atmosphere Models. London: Elsevier, 543–590

Xia Ruibin, Liu Chengyan, Cheng Chen. 2018. On the subtropical Northeast Pacific mixed layer depth and its influence on the subduction. Acta Oceanologica Sinica, 37(3): 51–62, doi: 10.1007/s13131-017-1102-3

Xia Ruibin, Liu Qinyu, Xu Lixiao, et al. 2015. North Pacific Eastern Subtropical Mode Water simulation and future projection. Acta Oceanologica Sinica, 34(3): 25–30, doi: 10.1007/s13131-015-0630-y

Xie S-P, Deser C, Vecchi G A, et al. 2010. Global warming pattern formation: sea surface temperature and rainfall. Journal of Climate, 23(4): 966–986, doi: 10.1175/2009JCLI3329.1

Xu Lixiao, Li Peiliang, Xie S-P, et al. 2016. Observing mesoscale eddy effects on mode-water subduction and transport in the North Pacific. Nature Communications, 7(1): 10505, doi: 10.1038/ncomms10505

Xu Lixiao, Xie S-P, Liu Qinyu. 2012. Mode water ventilation and subtropical countercurrent over the North Pacific in CMIP5 simulations and future projections. Journal of Geophysical Research: Oceans, 117(C12): C12009

Xu Lixiao, Xie S-P, Liu Qinyu, et al. 2017. Evolution of the North Pacific subtropical mode water in anticyclonic eddies. Journal of Geophysical Research: Oceans, 122(C12): 10118–10130

Zhang Ruosi, Xie S-P, Xu Lixiao, et al. 2016. Changes in mixed layer depth and spring bloom in the Kuroshio Extension under global warming. Advances in Atmospheric Sciences, 33(4): 452–461, doi: 10.1007/s00376-015-5113-8